A&A manuscript no.
(will be inserted by hand later)

Your thesaurus codes are:
11 (11.03.1; 11.03.4 MS2255.7+2039; 11.05.2; 11.06.1; 11.12.2; 12.03.3)

ASTRONOMY AND ASTROPHYSICS

The Luminosity Function of MS2255.7+2039 at $z = 0.288^{\star}$

Magnus Näslund, Claes Fransson, and Monica Huldtgren

Stockholm Observatory,
SE-133 36 Saltsjöbaden,
Sweden

Received; accepted

Abstract. The luminosity function of MS2255.7+2039 at $z = 0.288$ is determined down to a total magnitude of $R \sim 24$, corresponding to $M_{\rm R} \sim -17$ ($\rm H_0 = 50$ km s^{-1} Mpc^{-1}). The data are corrected for incompleteness and crowding using detailed simulations. We find that the luminosity function is steeper than a standard Schechter function at faint magnitudes, and shows an excess of galaxies below $M_{\rm R} \sim -19$. After corrections for light loss and crowding, the data can be described by a sum of two Schechter functions, one with $M^*_{\rm R} = -22.8$ and $\alpha = -1.0$, and one steeper with $M^*_{\rm R} = -18.9$ and $\alpha = -1.5$, representing the dwarf population. A straight-line fit to the faint part yields a slope similar to the Schechter $\alpha = -1.5$ of the dwarf population. The luminosity function of MS2255.7+2039 is compared to other clusters at lower redshifts, and does not show any significant difference. The redshift range for clusters in which increased number of dwarf galaxies have been found is therefore extended to higher redshifts.

Key words: Galaxies: clusters: general – Galaxies: clusters: individual: MS2255.7+2039 – Galaxies: evolution – Galaxies: formation – Galaxies: luminosity function, mass function – Cosmology: observations

1. Introduction

The faint end of the luminosity function (LF) is of great interest both in connection to the excess found in number counts of faint galaxies and for theories of cluster formation. The latter is demonstrated especially in a series of papers by Kaufmann et al. (1993), Kaufmann (1995a, b), Heyl et al. (1995) and Baugh et al. (1996), which show how the LF is related to the hierarchical clustering in e.g. the Cold Dark Matter (CDM) model. A steep faint end of the LF is unique not only to the CDM scenario, but is a generic prediction of hierarchical models of cluster formation (White & Frenk 1991). The difference of the LF in the field and in clusters of galaxies also gives important information about environmental effects related to the galaxy formation process. In particular, ram pressure stripping and effects of interaction are likely to be more important for clusters than in the field (e.g., Moore et al. 1996). There is in this respect a clear connection to the Butcher-Oemler effect (Butcher & Oemler 1984), seen for clusters, but not apparent in the field. The fraction of blue galaxies in clusters is larger at higher redshifts, which is often interpreted as an evolutionary effect. The evolution of the cluster LF is therefore of obvious interest.

The field LF has been investigated locally by several groups. Some of these report local LFs with flat faint-end slopes of $-1.1 \lesssim \alpha \lesssim -1.0$ (Loveday et al. 1992; Ellis et al. 1996), while others have found a significantly steeper LF with $\alpha \lesssim -1.5$ (Marzke et al. 1994; Lilly et al. 1995). At higher redshifts especially the CFRS survey (Lilly et al. 1995) and the Autofib survey (Ellis et al. 1996) give information about the LF in the field up to $z \sim 1$. Lilly et al. find that, while strong evolution is seen for the blue sample at $z \gtrsim 0.5$, the red LF is changing little. At $z \sim 0.5$ the LF has brightened by ~ 1 magnitude in B. At higher redshifts the bright end stays constant, while the faint continues to increase, leading to a steepening of the faint end of the LF, from $\alpha = -1.1$ locally to $\alpha = -1.5$ at $z \simeq 0.5$, in broad agreement with the Autofib survey. A steepening of the LF can explain the excess counts found in deep surveys, as discussed by Gronwall & Koo (1995).

While the field LF has been studied in fair detail, there have been only a few CCD investigations of the LF of clusters of galaxies until recently. Relatively nearby clusters, like Virgo, Fornax and Coma, have been studied by a number of authors (e.g., Bernstein et al. 1995, hereafter BNTUW; Lobo et al. 1997; Biviano et al. 1995; De Propris et al. 1995; Trentham 1998a). While some earlier investigations yield faint-end slopes of $\alpha \simeq -1.3$ (e.g., Ferguson & Sandage 1988), more recent investigations, taking low surface brightness galaxies into account, point to steeper slopes, $\alpha \lesssim -1.5$ (e.g., Bothun et al. 1991).

* Based on observations made with the Nordic Optical Telescope, operated on the island of La Palma jointly by Denmark, Finland, Iceland, Norway, and Sweden, in the Spanish Observatorio del Roque de los Muchachos of the Instituto de Astrofisica de Canarias.

Correspondence to: magnus@astro.su.se

At higher redshifts the information about the cluster LF is scarce. The first detailed study was that by Driver et al. (1994b, henceforth DPDMD), who studied the R-band LF to $R = 24$ for the cluster Abell 963 at $z = 0.206$. While the high luminosity end can be well fitted with a Schechter function, they found an increase of faint galaxies between $-19 \lesssim M_{\rm R} \lesssim -16.5$, with a slope of $\alpha \simeq -1.8$. Further investigations at $0.1 \lesssim z \lesssim 0.2$ have strengthened the case for steep slopes, $\alpha \lesssim -1.7$, at $-19 \lesssim M_{\rm R}$ (Smith et al. 1997; Wilson et al. 1997, hereafter WSEC), although examples of flatter LFs also exist (Trentham 1998b).

It is obvious that these results need confirmation for more clusters, especially at higher redshifts. Because of the strong evolution of the Butcher-Oemler effect, as well as from numerical simulations of cluster evolution (e.g., Kauffmann 1995a,b), one expects substantial evolution even from $z = 0.2$ to $z = 0.4$. The detection of the faint end of the LF then becomes more difficult, both because the galaxies are fainter, and because of increasing contamination from the background. As a first step we here report observations of the cluster MS2255.7+2039 at $z = 0.288$. We will in this paper use $\rm H_0 = 50$ km s^{-1} Mpc^{-1} and $\Omega_{\rm M} = 1$.

2. The data

The coordinates of the center of MS2255.7+2039 = Zw 8795, hereafter MS2255, are $\alpha = 22^{\rm h}\ 55^{\rm m}\ 40\overset{\rm s}{.}6$, $\delta = 20^\circ\ 30'\ 04\overset{''}{.}2$ (1950.0), and the redshift is $z = 0.288$ (Stocke et al. 1991). MS2255 was detected as an X-ray cluster in the Einstein Observatory Extended Medium Sensitive Survey (EMSS), with an X-ray luminosity of 2.0×10^{44} erg s^{-1} in the $0.3 - 3.5$ keV band (Gioia & Luppino 1994), fairly typical for the EMSS selected sample.

The galactic extinction can be estimated in several ways. Based on the H I column density, the absorption in the direction of MS2255 ($l = 90\overset{\circ}{.}32, b = -34\overset{\circ}{.}67$) is $A_{\rm B} = 0.18$ (Burstein & Heiles 1982). With $A_{\rm R} = 0.61\ A_{\rm B}$ we get $A_{\rm R} = 0.11$. On the other hand, the estimated X-ray column density is 5.0×10^{20} cm^{-2} (Gioia et al. 1990). With $N_{\rm H} = 4.8 \times 10^{21}\ E_{\rm B\text{-}V}$ (Bohlin et al. 1978) and $A_{\rm R} = 2.4 E_{\rm B\text{-}V}$ this gives $A_{\rm R} = 0.25$, considerably higher than the value deduced from the H I column density. Finally, the recently presented COBE/DIRBE - IRAS/ISSA dust maps (Schlegel et al. 1998) yield $E_{\rm B\text{-}V} = 0.06$, which leads to $A_{\rm R} = 0.14$. We will in this paper use $A_{\rm R} = 0.14$, but note that this may be in error by ~ 0.1 magnitude.

2.1. Observations

The data were obtained with the 2.56 m Nordic Optical Telescope and the Andalucia Faint Object Spectrograph (ALFOSC) in June 1997. The ALFOSC contained a thinned, back-side illuminated Ford-Loral 2K^2 chip that yielded a field of $6\overset{'}{.}5 \times 6\overset{'}{.}5$ and an image scale of $0\overset{''}{.}189$/pixel. Every data set consists of the usual bias, dark, twilight-flatfield, and standard-star images, beside the science frames.

To determine the LF of the cluster it is crucial to correct for the contribution from the field. A nearby field at $\alpha = 22^{\rm h}54^{\rm m}55\overset{\rm s}{.}04, \delta = 21^\circ 32' 19\overset{''}{.}00$ (1950.0) was chosen in order to have similar galactic latitude and extinction properties as the cluster. Furthermore, the seeing conditions during the observations turned out to be similar. All these factors are crucial to ensure that the foreground and background will be as similar to the cluster field as possible. Systematic errors may otherwise easily enter into the subtraction of the background.

The total exposure time was 5400 seconds for both the cluster and the background field, respectively, divided into exposures of 900 seconds. During the observations we rotated the instrument by 90° and/or made offsets by 10″ between different frames. This was done in order to suppress the influence of bad regions on the chip and to make it possible to create a night-sky flatfield from the object frames (e.g., Tyson 1988). A pointing error of the telescope at the time of the observations may have caused the centre of the cluster and the image field centre to differ slightly.

2.2. Reductions

The bias level was determined from the overscan of each frame. These values were used to scale a master bias that was subtracted from the frames. We then used the shifted, bias-subtracted science frames to create a night-sky flatfield by removing objects with a 'smooth-and-clip' (Näslund 1995), followed by an averaging of the frames. We corrected the large-scale gradients of the twilight flatfield by the night-sky master flat, and used the corrected twilight flatfield to flat the science frames.

A narrow strip along the edges had to be excluded in the frames due to the structure of the thinned CCD. The flat-fielded frames were sky-subtracted, corrected for atmospheric extinction, aligned and finally combined (see Näslund 1995). The rotation and shifting of the frames decreased the effective area of the combined image, so that the area of the background and cluster images became $5\overset{'}{.}6 \times 5\overset{'}{.}5 = 31.0\Box'$ and $5\overset{'}{.}4 \times 5\overset{'}{.}6 = 30.2\Box'$, respectively (the final detection areas were reduced somewhat in order to avoid edge effects; see below). The images were calibrated using standard stars observed at intervals during the night. The seeing in the combined images was in both cases $0\overset{''}{.}85$ (FWHM). The background field is shown in Fig. 1, while Fig. 2 displays the cluster.

The individual frames of the cluster and background fields were checked for 'internal consistency'. We selected a few common objects in the magnitude range 17-21 and determined their brightness both in FOCAS (Jarvis & Tyson 1981; Valdes 1982, 1993) and DAOPHOT (Stetson 1987). All objects were consistent within a few hundredths of a

Fig. 1. The $5\farcm6 \times 5\farcm5$ background field image in the R band. The total exposure time is 5400 seconds.

magnitude or better. The weighted average of the standard stars observations yielded an statistical uncertainty of ± 0.01 magnitude.

3. Analysis of the fields

3.1. Object catalogue

The reduced fields were analyzed using the FOCAS package. As a limit to our detections we used a value of 2.5σ of the sky noise and a detection area A of 20 pixels, which corresponds to the seeing. We then utilized the ordinary FOCAS procedure, including sky correction and splitting of multiple objects. The splitting procedure was checked by simulations and worked satisfactory in most cases. A region of 50 pixels along the edges was excluded when counting galaxies, which decreased the effective area of the background field to $27.65\square'$ and of the cluster field to $27.02\square'$. This procedure resulted in a catalogue of objects with a number of parameters such as isophotal R magnitudes ($m_{\rm R}^{\rm iph}$) and intensity weighted first-moment radii (r). A plot of the detected galaxies is shown in (Fig. 3).

3.2. Simulations

A substantial part of the analysis consists of simulations in order to determine completeness levels, fraction of noise detections, and magnitude corrections. When we approach the level of the sky noise we will obviously lose some galaxies in the noise, as well as pick up false detections. This problem is for a given total magnitude most severe for galaxies with large scale lengths and therefore low surface brightness. As discussed by, e.g., DPDMD and WSEC, the determination of this factor is far from trivial, and unfortunately, model-dependent assumptions about the galaxies are necessary. In one approach, discussed by DPDMD, one generates artificial galaxies with fixed parameters shifted to different redshifts, to describe the surface brightness distribution. An alternative method, used by WSEC, is to use real galaxies at brighter magnitudes, typical for the population in the field, as templates, and then rescale these to fainter magnitudes. This approach has the advantage of using realistic brightness profiles. It, however, implicitly assumes that the relative fractions of the different morphological types are the same for faint magnitudes as for bright, and also that the brightness profiles of a given type is independent of luminosity, except for a normalization factor. Neither of these assumptions are obvious.

We used a generalized version of the DPDMD method in this investigation; the objects were not only characterized by their brightness, but also by their scale size. Simulated exponential disks were added to the background-field image, and these artificial galaxies were then detected with the same criteria as were used for the real data. After detection we could determine the magnitude correction depending on the objects position in the magnitude-scale length diagram (see Section 3.2.3).

3.2.1. Noise simulations

First, a number of Poisson-noise frames were created, with a noise level corresponding to that of the data. We then used FOCAS to detect spurious features with different combinations of the upper sigma limit and detection area. The parameters we settled for, $\sigma = 2.5$ and $A = 20$ pixels ($\approx$ seeing), yielded six noise detections in an area of $27\square'$. This amounts to about 0.2% of the actual detections in the background field.

3.2.2. Completeness

To estimate the completeness we simulated exponential disks of different magnitudes, scale lengths and inclinations. For each set of parameters, 51 exponential disks were generated in empty regions of the background-field image. The reason for positioning the simulated galaxies in empty regions was to isolate the detection completeness due to surface brightness, and treat other effects, like overlapping (cf. Section 3.2.4), separately. We used FOCAS with the same detection criteria as for the real data. The parameters of the detected artificial objects could then be extracted from the resulting catalogue. As mentioned below, and discussed by other authors (DPDMD, Trentham 1997), the possibility of detection, as well as the fraction of the total light recovered, varies with surface brightness, which in turn depends on scale length and inclination for a given magnitude. At fainter magnitudes, galaxies with

Fig. 2. R-band image of MS2255.7+2039. The field covers $5\farcm4 \times 5\farcm6$ and the total exposure time is 5400 seconds. North is up and East is to the left.

short scale length are, as expected, more easily detected than those with long scale lengths. The simulations indicate that we detect all dwarf galaxies, modelled as exponential disks ($0.5 \lesssim r_{\rm d} \lesssim 2$ kpc, where $r_{\rm d}$ is the disk scale length), down to $R \sim 25$.

An important complication is the possible presence of low surface brightness galaxies (LSBGs). These come in different flavours, such as the sample of blue Low-Surface-Brightness Galaxies of McGaugh & Bothun (1994) and the Giant Low-Surface-Brightness Galaxies of Sprayberry et al. (1995). The central surface brightness distribution of galaxies is not well known, although research during the last decade has shed more light on this particular type of object (Impey & Bothun 1997). If LSBGs are peaked around $\mu_{\rm B}^0 \simeq 23.2$ mag/$\Box''$(corresponding to $\mu_{\rm R}^0 \simeq 22.0$ mag/$\Box''$), as those observed by Sprayberry et al. and McGaugh & Bothun, we would detect LSBGs with small and intermediate scale lengths ($r_{\rm d} \sim 3$ kpc), given the colours of the Sprayberry et al. sample. Even objects with lower surface brightness, like UGC 9024 ($\mu_{\rm B}^0 = 24.5, r_{\rm d} = 5.6/h$ kpc), should be possible to detect at $z = 0.288$, although such galaxies are close to our detection limit. Galaxies with lower surface brightness will accordingly escape detection. The most extreme cases known (e.g. Malin 1) are far beyond detection, but galaxies of this type are likely to be an order of magnitude fewer than objects of higher surface brightness (Davies et al. 1994). Furthermore, a study of Hubble Deep Field data by Driver (1999) shows that luminous low surface brightness galaxies are rare compared to their high surface brightness counterparts. One should, in any case, bear in mind that LSBGs below the surface-brightness detection limits may influence the faint-end slope by an unknown amount.

3.2.3. Magnitude correction

From the simulations above, used to determine the completeness, we also estimated the total magnitude for each parameter set. During the analysis we developed a technique for magnitude corrections (Näslund 1998), which turned out to be similar to that of Trentham (1997). A large number of simulated galaxies, with different values

of scale length ($r_{\rm d}$), axial ratio (b/a) and total magnitude ($m_{\rm R}^{\rm tot}$), were generated in the background-field image. These objects were detected with the same setup as for the real data. We could at this stage calculate the magnitude correction as a function of isophotal magnitude ($m_{\rm R}^{\rm iph}$) and intensity weighted first-moment radius (r). We, finally, corrected the magnitudes of the detected galaxies from their position in the $(m_{\rm R}^{\rm iph}, r)$ plane (Fig. 3).

This method will obviously not be fully correct for elliptical galaxies that are better described by de Vaucouleur profiles than by exponential disks. Most of these are, however, of comparatively bright magnitudes, where the correction is small. If we assume that the faintest cluster members, for which the corrections are largest, have exponential profiles the application of the method is justified. This is plausible if the faintest galaxies are late-type spirals or dwarf spheroidals and/or dwarf irregulars. However, some of the galaxies close to our magnitude limit ($R \sim 24$) may be *luminous* dwarf ellipticals ($-16 < M_{\rm B}$) that are better fitted by de Vaucouleurs profiles (Ferguson & Binggeli 1994). We performed a few simulations of de Vaucouleurs profiles with short scale lengths to mimic luminous dwarf ellipticals, and compared them to exponential disks of the same brightness. We find that the total magnitudes for the $r^{1/4}$ profile galaxies are underestimated by 0.15 magnitudes, similar to the findings of Trentham (1997).

The magnitude correction can be applied in two ways. One can either correct for 'light loss' without any assumptions about the cluster population, or one may use *a priori* information to constrain the distribution of points in the $(m_{\rm R}^{\rm iph}, r)$ plane. If the faintest cluster members that we detect are exclusively dwarfs, this has two implications. Firstly, for objects with $r_{\rm d} \lesssim 2$ kpc the catalogue should be more than 50% complete for $m_{\rm R}^{\rm iph} < 26$. Secondly, the magnitude correction would in this case be fairly small, and the ambiguity at the faintest magnitudes is reduced, compared to a more complex population. This is because faint galaxies are found in a comparatively small region of the $(m_{\rm R}^{\rm iph}, r)$ plane, and the reason is simply that faint, intrinsically large galaxies (i.e. LSBGs), will have their apparent scale lengths substantially reduced, and thereby be closer to the true dwarf region of the $(m_{\rm R}^{\rm iph}, r)$ plane. As a result, the uncertainties in the magnitude correction increase at the faint end. If one for good reasons could justify the exclusion of non-dwarfs from this region of the $(m_{\rm R}^{\rm iph}, r)$ plane, the corresponding magnitude correction would be more accurate. In addition, if all faint galaxies are dwarfs and have $r^{1/4}$ profiles, the luminosity after correction would be systematically underestimated (see above). On the other hand, if they *all* are luminous dwarf ellipticals the magnitude correction would not be increasing with magnitude as steeply as the one applied here, and the LF would therefore be less steep at faint magnitudes. However, there is no strong motivation for such an exclusion of intrinsically larger objects, and for the data presented here we used the first, more general, approach. The possible presence of larger, faint objects also calls for the use of exponential profiles.

Fig. 3. The detected galaxies in the $(m_{\rm R}^{\rm iph}, r)$ plane of the cluster image. $m_{\rm R}^{\rm iph}$ is the isophotal R-band magnitude and r the intensity weighted first-moment radius.

The magnitude-correction procedure was tested by generating a number of exponential disks distributed in magnitude according to a power law of slope 0.4. The galaxies were positioned along a grid in order to avoid crowding effects in this particular test. The simulations showed that the procedure managed to correct for the light loss well down to $R \simeq 24$, close to the actual completeness limit (for $r_{\rm d} \lesssim 6$ kpc) of the data (Näslund 1998).

3.2.4. Crowding

Overlapping objects is another important factor, especially for faint objects. One way to see this is by noting that fainter objects have smaller effective field areas at their disposal. Stars and galaxies that are brighter in general occupy a larger apparent area in the image and fainter objects are shielded by them.

We have tested different methods for this correction. In the first approach we added simulated compact objects of different magnitudes to the cluster and background images. To a first approximation, the fraction of recovered objects gives the detection probability as a function of magnitude. However, non-linear effects, connected with obscuration between especially the faint galaxies themselves, are likely to be important, and full simulations of the cluster and background would be needed to address these aspects.

Instead of this method we adopted a more conservative correction procedure for the obscuration of faint objects. The cumulative area covered by objects up to a certain magnitude was calculated in half-magnitude intervals for the background and cluster field, respectively. It was then found that there is a clear difference between the area covered in the cluster image and the background - field image when it comes to *bright* objects. However, for fainter objects there is no substantial difference; the covered area increases similarly in both fields. In practice, this means that for objects brighter than $R \sim 22$ the obscured area is 8% in the cluster image, while the corresponding number for the background image is only 3.4%. We accordingly used these numbers to correct for the obscuration for objects fainter than $R = 22$. We do therefore not include any magnitude dependence of the correction factor below $R = 22$, as Smith et al. (1997) do, which implies that apparently small objects are not an important source of obscuration in our fields. Furthermore, these effects do not add linearly with brightness for faint objects. In the case that faint objects contribute somewhat themselves to the obscuration, we would have underestimated the faint - end slope of the LF slightly. We hope to perform a more thorough study of crowding effects elsewhere.

3.3. Foreground and background corrections

3.3.1. Stars

MS2255 is at comparatively low galactic latitude ($b = -34\overset{\circ}{.}67$), and a substantial contamination by stars is expected. Because our comparison field is close to the cluster, this contamination is to a large extent reduced when we subtract the background counts from the cluster counts. With FOCAS, we can nevertheless separate stars from galaxies, based on the brightness profile, for $R \lesssim 20$. This eliminates the statistical errors in the cluster counts from this source. The saturated stars were removed interactively from the galaxy list, while remaining stars brighter than $R = 20$ were detected and classified by FOCAS. We found in this way 25 stars in the cluster field, and 17 in the background field. This can be compared to the number expected from the galactic model by Bahcall & Soneira (1980) and Bahcall (1995), which for a field of 27 $\Box'$ gives 30 stars brighter than $R = 20$. Within the statistical errors we consider the number of stars in the cluster field to be consistent with that expected from the model. The lower number for the background field is simply explained by the fact that the field was selected in a region void of bright objects.

Besides bright stars, we also excluded small spurious objects around bright stars or galaxies, which can be a result of false detections by FOCAS in the cluster and background field (see Trentham 1997 for a discussion). This effect does not affect the faint-end slope significantly.

3.3.2. Background counts

Guided by the completeness simulations, we decided to set the isophote limit for inclusion in the catalogue at $m_{\rm R}^{\rm iph} = 26$, approximately corresponding to the magnitude limit after correction given above. According to the simulations we detect all pointlike sources at this isophotal magnitude.

Inspection of the $(m_{\rm R}^{\rm iph}, r)$ plane shows that some of the detected objects fall below the simulated point sources, i.e. they have scale lengths smaller than the seeing. The apparent small scale length may be a result of the small number of counts (ADUs) for the faint objects. There is then a substantial probability that even for a point-like object the scale length will be smaller than the width of the PSF. Moreover, the simulations showed that disks with large scale lengths that are below the completeness limit could be detected as such compact objects, but almost all of them have $m_{\rm R}^{\rm iph}$ beyond our catalogue limit anyway, and hence cause no problem. The ambiguity in the interpretation of the nature of these objects made us test whether they influenced the shape of the cluster LF. We generated one list that included these objects, and one in which they were removed for both the cluster image and the background-field image. The resulting faint-end slope is in the latter case somewhat flatter compared to the slope including these objects, which is the one presented in this paper.

In Fig. 4 we show the corrected R - band background counts, together with those obtained by the Hitchhiker team at WHT (Driver et al. 1994a) and the counts from BNTUW. As seen in the figure, the corrected background counts agree well with each other down to $R \sim 24$, within the limited statistics. While we have a total background area of $27.65\Box'$, Driver et al. had a total area of $15.9\Box'$. Their exposures with the WHT were, however, deeper in these fields. We also note that our counts are within the variations of other recent investigations such as those by Arnouts el al. (1999) and Fontana et al. (1999).

4. The cluster luminosity function

4.1. Error estimation of cluster counts

Because of both statistical and systematic errors a careful error analysis has to be made. The standard method has been to assume Poisson statistics for the galaxies in the background field and cluster field, respectively, in some cases supplemented by an error for the field - to - field variation caused by large scale structures. Because we have only one background field, we cannot determine the field-to-field variation from our material. We therefore use the field - to - field statistics of BNTUW, with the characteristics of our data, to estimate the variation in the background counts as a function of magnitude (see also Trentham 1997). This value was added in quadrature to the Poisson variation in the cluster counts and the error due to the magnitude correction. The latter was estimated as

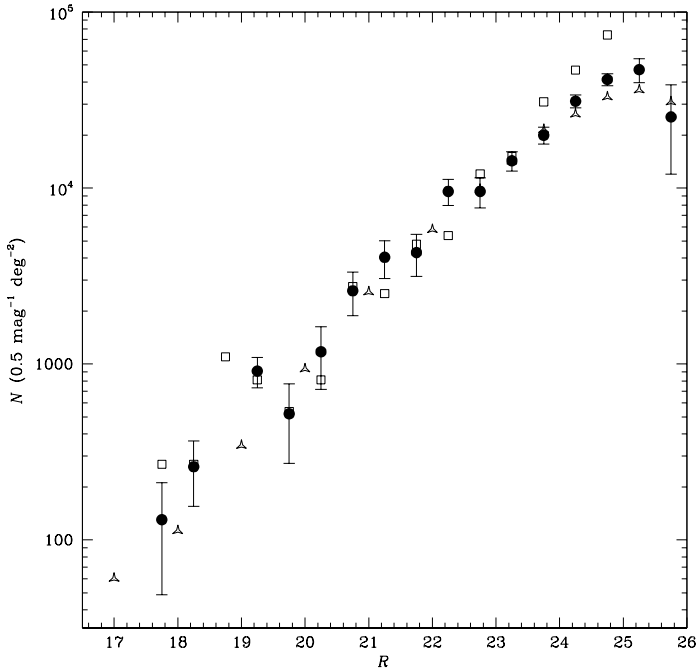

Fig. 4. Differential number of galaxies as a function of isophotal R-magnitude for the background field (filled circles). The background counts of DPDMD (open squares) and BNTUW (open triangles) are also shown.

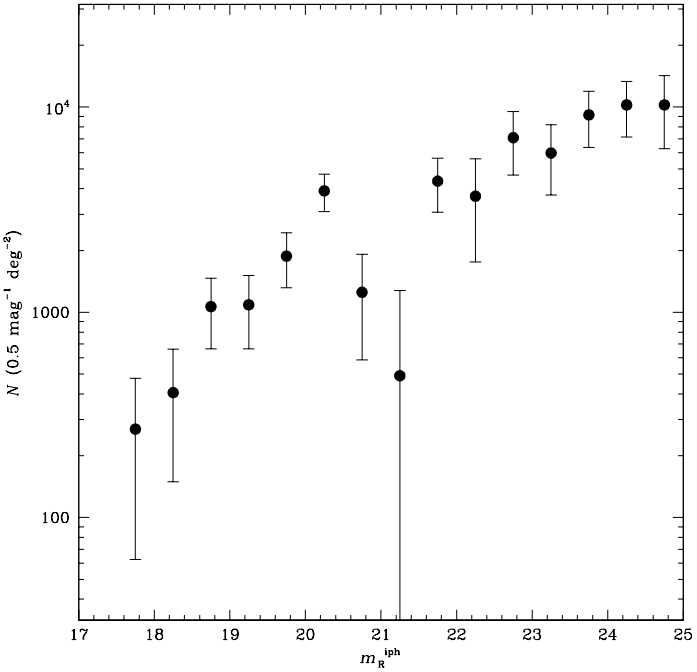

Fig. 5. Background-subtracted differential number of galaxies per 0.5 mag and square degree as a function of isophotal R-magnitude for MS2255.7+2039. No corrections have been applied.

the 1σ dispersion in a number of simulations (see Section 3.2.3). The two error sources are generally of comparable magnitude, but the field-to-field variation is systematically larger for fainter magnitudes ($R > 22.5$).

4.2. The raw LF

By subtracting the background counts from the cluster counts, we obtain the LF in terms of the apparent, isophotal magnitude. This 'raw' LF is shown in Fig. 5. Then we applied the same distance modulus, including K-correction, as for the corrected distribution (see below). The resulting distribution can be fitted by a single Schechter function with $\alpha = -1.4$ and $M_{\rm R}^* = -24$. It is important to note that these numbers are arrived at partly because of the two 'low' bins at $M_{\rm R} = -20.75$ and $M_{\rm R} = -20.25$. If we exclude these points, we obtain $\alpha = -1.3$ and $M_{\rm R}^* = -22.8$. Although the shape of the LF suggests that the bright end would be better fitted by a Gaussian, these low values can be explained as a statistical effect. Both points are fitted within the 2σ level by a Schechter function with parameters $M_{\rm R,giants}^* = -22.5$, $\alpha = -1.0$ (see Fig. 7). Monte Carlo simulations of this Schechter function with the same total number of galaxies as observed, show that a dip similar to that in Fig. 5 appears in $(10 - 20)\%$ of the simulations. We therefore conclude that this dip is of marginal significance.

The Schechter parameters can be compared to those of Valotto et al. (1997), who found $\alpha = -1.4$ for rich clusters and $\alpha = -1.2$ for poor. A linear fit for the range $-19 < M_{\rm R} < -17$ also yielded $\alpha = -1.3$, which is the least model dependent estimate of the uncorrected faint-end slope. A comparison of 'raw' LFs at different redshifts is, however, misleading.

4.3. The corrected LF

For an unbiased comparison with samples at other redshifts, the isophotal magnitudes have to be related to the total magnitude, and then translated into absolute magnitudes. For the latter we included an R-band K-correction given by Metcalfe et al. (1991), who found a K-correction of 0.41 magnitudes for E/S0 galaxies at $z = 0.288$, while the average for spirals was 0.09. We used a straight mean value $K = 0.15$, but realize that the true range may be $-0.1 \lesssim K \lesssim 0.41$. Because of the type dependence of the K-correction the intrinsic cluster LF is expected to be slightly redistributed, compared to the one observed. This redistribution should, however, be within the limits just mentioned. Thus, the distance modulus became $(m - M) = 41.47 - K$.

In order to estimate the influence of the K-correction on the measured slope we made two tests. In both cases we kept the correction of the bright population fixed at $K = 0.15$, but applied values of $K = 0.1$ and $K = 0.4$, respectively, to the dwarfs. This was done by simply assuming that all bins in the LF at $R > 23$ represent the dwarf population, since this is the region where the dwarfs

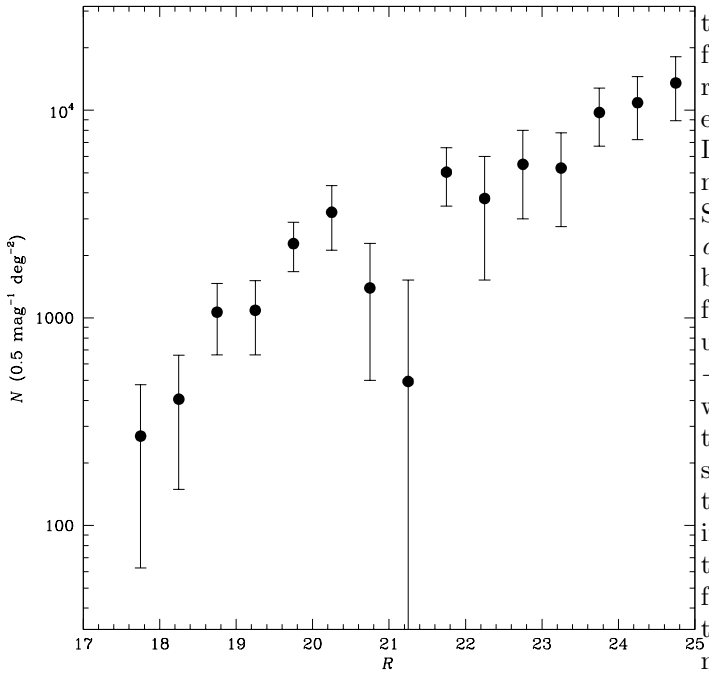

Fig. 6. Background-subtracted and corrected differential number of galaxies per 0.5 mag and square degree as function of isophotal R-magnitude for MS2255.7+2039.

dominate in the corrected LF (see Fig. 7). In neither case is the faint-end slope for the the fitting method described below affected.

The uncorrected LF presented in Section 4.2 represents a strict lower limit to the true LF. By applying the magnitude and crowding corrections, described in previous sections, to the cluster field and background field, respectively, we arrive at the LF shown in Fig. 6.

While providing a useful description of the data, a Schechter fit is not unique, and we have tested different parametrizations of the corrected data. A single Schechter function with $M^*_{\rm R} = -23.9$ and $\alpha \simeq -1.43$ gives a decent fit, although there is an indication of a break at $M_{\rm R} \simeq -20$.

Binggeli et al. (1988) discussed the separation of the total LF into components for each Hubble type for the Virgo cluster. This is not possible for our data, because of the distance to the cluster, the lack of colour information, etc. We can, however, use the *a priori* information that the transition region between giants and dwarfs is at $-18 \lesssim M_{\rm B} \lesssim -16$. For comparison reasons, we add two separate Schechter functions, one representing giant galaxies and the other representing dwarfs. If the slope of the giants is fixed at $\alpha = -1.0$, the procedure yields $M^*_{\rm R,giant} = -22.8$ and $M^*_{\rm R,dwarf} = -18.9$ for the two populations. This is close to the corresponding values found by DPDMD $(-22.5, -19.0)$. The main discrepancy is in the slope of the dwarf population. For MS2255 we find $\alpha \simeq -1.5$. This can be compared to A963 for which DPDMD find $\alpha \simeq -1.8$. It is, however, important to note the coupling between M^* and α. For $M^*_{\rm R,dwarf} = -19.5$ our faint-end slope yields $\alpha \simeq -1.8$, while $M^*_{\rm R,dwarf} = -18.5$ results in $\alpha \simeq -1.2$ (the dwarf/giant ratio was, however, not constrained in these tests, as in the case of DPDMD's fit). The strong coupling between α and $M^*_{\rm R}$ makes it dangerous to draw any firm conclusions based on Schechter-function fits only. Instead, *one should directly compare any two LFs, magnitude by magnitude*, as shown below. In order to avoid the coupling of the Schechter-function parameters for the faint end of the LF, we also used a simple straight-line fit to the last five data bins, $-19.5 \leq M_{\rm R} \leq -17$ (as proposed by Trentham 1998b), which yielded $-1.6 \lesssim \alpha \lesssim -1.5$. This is somewhat steeper than the 'raw' LF, and is caused by the magnitude and obscuration corrections. This steepening of the LF is consistent with the bright end of the dwarf population detected in more nearby clusters (see discussion below). Although the procedures discussed above yield a formal value of the faint-end slope of $\alpha \simeq -1.5$, the uncertainties involved in these kind of studies make us emphasize that one should not focus on the exact value of the slope, but rather on the qualitative appearance of the LF.

4.4. Comparison with other clusters

A major reason for the interest in the cluster LF is to study the evolutionary effects with redshift. As we have just discussed, this is done best by a direct comparison of the different LFs, i.e. by plotting them together, including all corrections. A problem is that the observations are in different filters and/or that the K-corrections are uncertain. A possibility to avoid some of these uncertainties is to compare the LFs in filters with central wavelengths adjusted to the redshift. In our case we note that at $z = 0.288$, the R band corresponds to a wavelength between B and V at $z = 0$. The other, more model dependent, method is to use a K-correction for a given z and a given filter. This depends, however, on the population (section 4.3), as well as on evolution. Unfortunately, we are in most cases forced to use this alternative.

In Fig. 7 we display the LF for MS2255 together with Trentham's (1998a) LF of Coma ($z = 0.023$) and the LF of A963 ($z = 0.206$) by DPDMD, all adjusted to $\rm H_0 = 50$ km s^{-1}Mpc^{-1}. Both LFs were normalized to the same level as MS2255 for galaxies brighter than $M_{\rm R} = -21$. Although a fainter limit for this normalization would have been preferable, this value was chosen to avoid influence from the low points in the LF of MS2255 at $M_{\rm R} \simeq -21$.

It is evident that all three clusters exhibit steep slopes at the faint end, and there is accordingly no qualitative difference between nearby and distant clusters in that respect. The slope of Coma is actually as steep as that of A963, while MS2255 displays a somewhat flatter faint end of the LF. The steep slope of the Coma LF was also noted by Smith et al. (1997), who used Coma data from Thompson & Gregory (1993). The steepening occurs at slightly

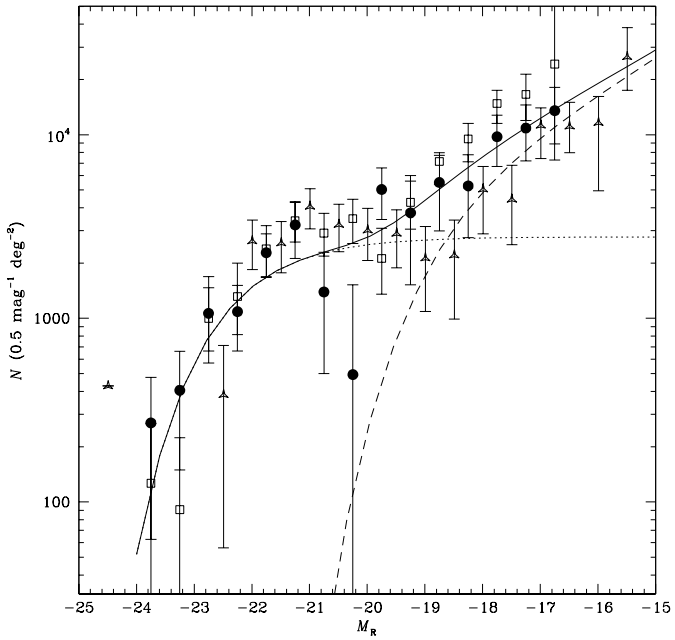

Fig. 7. Luminosity functions of three galaxy clusters. Filled circles represent MS2255.7+2039, open squares A963 (DPDMD), and open triangles Coma (Trentham 1998a). A963 and Coma have been normalized to MS2255.7+2039 for $M_{\rm R} \leq -21$. The curve represents a combination of two Schechter functions ($M^*_{\rm R,giants} = -22.5$, $\alpha = -1.0$, dotted line; $M^*_{\rm R,dwarf} = -19.0$, $\alpha \simeq -1.5$, dashed line) and is shown here in order to guide the eye.

different magnitudes. A963 has its break point around $M_{\rm R} = -19.5$. The steepening in MS2255 starts at approximately the same magnitude, while that in Coma occurs at a somewhat fainter magnitude ($M_{\rm R} \simeq -18.5$).

The shape of the faint end of the cluster LF is a matter of controversy. While both nearby and more distant clusters show a steepening of the LF, the magnitude where this occurs differs substantially. To some extent this may be caused by a simple zero-point shift between filters. Most studies at intermediate redshifts ($0.1 \leq z \leq 0.2$) yield steep slopes ($-2 \lesssim \alpha \lesssim -1.7$) for $-19 \lesssim M_{\rm R}$ (DPDMD; Smith et al. 1997; WSEC). However, the studies by Trentham (1998b, c), which in some cases are based on local clusters, give a more shallow slope ($\alpha \simeq -1.4$). In some local clusters, the steep slope starts at $M_{\rm R} \simeq -14$, which is a region beyond the limits of present studies for clusters around $0.2 \lesssim z \lesssim 0.3$. One reason for the discrepancies can be the different correction methods applied. It should be noted that earlier photographic investigations of nearby clusters also suffered from severe selections effects that work against low surface brightness objects. When such effects have been corrected for, the resulting slope is in the range $-1.5 \lesssim \alpha \lesssim -1.8$ (Impey et al. 1988; Bothun et al. 1991).

Another subject of interest is the possible existence of a universal cluster LF. In view of the discussion above, this is highly controversial and depends e.g. on the correction procedures applied. Composite LFs of clusters at $0.02 \simeq z \simeq 0.2$ have been presented both in B and in R, based on more than 15 (in B) and six clusters and groups (in R), respectively (Trentham 1998c, d). The composite R-band LF has a slope of $\alpha \simeq -1.5$ at $M_{\rm R} \simeq -17$, which is similar to what has been found here for MS2255. The steep slope of Coma (Trentham 1998a) seems to have been averaged out by the weighting procedure in the composite LF. Trentham noted, however, that his composite function may be valid only for the centres of rich clusters, i.e. regions dominated by ellipticals.

WSEC studied two clusters, A665 and A1689, both at $z = 0.18$, in V and I. This study is especially interesting because it gives some information about the colour dependence of the LF. WSEC found rising LFs with breaks around $M_{\rm V} = -19$ and $M_{\rm I} = -21$. Their V-band slope, after correction for incompleteness and obscuration, is very steep ($\alpha \sim -2$), while that in the I band is significantly flatter ($\alpha \sim -1.1$). This difference is interesting, since it indicates that the faintest detected galaxies indeed are blue. If this effect is real, one would expect an even steeper slope in B. Somewhat surprisingly, Trentham (1998b) did not find a comparatively steep B-band LF in his study of A665. Furthermore, while displaying very steep slopes ($\alpha < -2$), the four Abell clusters investigated by De Propris et al. (1995) did not show any differences between B and I in this respect. The question of colour dependent slopes is therefore still unanswered.

Few numerical simulations of cluster LFs exist. White & Springel (1999) discuss in a recent paper a combination of N-body and semianalytical modelling of the cluster population. Unfortunately, they only present the B-band LF, for which they find a faint end slope of $\alpha = -1.2$. Although a direct comparison is difficult (R at $z = 0.3$ corresponds approximately to V at $z = 0$), this is considerably flatter than the observed slope presented here.

5. Summary and conclusions

We have observed the galaxy cluster MS2255.7+2039 ($z = 0.288$) and a background field at similar galactic latitude with the aim of determining the cluster LF. The isophotal magnitudes have been corrected for light loss according to results obtained from simulations. We have also compensated for obscuration due to bright, apparently large, objects in the images. The resulting cluster LF has a fairly steep faint-end slope ($\alpha \simeq -1.5$) faintward of the break in the profile around $M_{\rm R} = -19$. This slope is more shallow than some LFs found in clusters both locally and at $z \simeq 0.2$, but similar to the slope of the composite LF derived by Trentham (1998c). Without focusing too strongly on the precise value of the slope, we conclude that MS2255.7+2039 exhibits a steepening LF at faint magnitudes.

The evidence for steep faint-end slopes of cluster LFs is accumulating. There are now a number of fairly deep CCD investigations of nearby, as well as a few medium distant ($z \lesssim 0.3$) clusters, that all point to rising LFs at faint magnitudes. It therefore seems clear that a flat LF (i.e., $\alpha = -1$) can be ruled out even at intermediate magnitudes ($-20 \lesssim M_{\rm R} \lesssim -17$). However, several questions remain unanswered. The uncertainties in the measured slopes are probably considerable, since different correction methods seem to yield deviating results, which probably explains the discrepancies between the LFs found for the same clusters as determined by different investigators (see section 4.4).

Because of these uncertainties, it is too early to discuss any variation of the faint-end slope with z. The accuracy of the present study only allows us to claim that the cluster LF is non-flat at faint magnitudes ($-19 \lesssim M_{\rm R}$). The exact values of the slope and the magnitude where the steepening sets in are uncertain, and any trend with z that may be present is dominated by these uncertainties. In addition, environmental differences, like richness or density, between clusters at the same z could affect individual LFs, making distinctions in z even more difficult to isolate. The uncertainties in the background subtraction is also a source of error, although the simulations by Driver et al. (1998) show that the faint-end slope of the LF can be reliably determined out to $z \simeq 0.3$ with seeing and depth similar to those of the present data. Nevertheless, the errors due to the statistical background subtraction can probably be substantially reduced by using photometric redshifts. Work based on this approach is in progress.

There are in the context of cluster LFs several important questions to answer in the future: Is there a universal LF for galaxy clusters at low redshifts, or is the steepness of the dwarf population different between clusters? Is there a colour dependence of the steepness of the dwarf population, as may be indicated in the study by WSEC? The K-band observations of five clusters by Trentham & Mobasher (1998) are especially interesting in this context. These data were, however, not deep enough to draw any conclusions about the faint end of the luminosity function. From the clear signs of evolution between $z = 0.5$ and the present epoch for the field (e.g., Lilly et al. 1995), one would expect a corresponding evolution in clusters. From the galaxy harassment scenario for the Butcher-Oemler effect (Moore et al. 1996) one may expect a larger fraction of low luminosity galaxies in the past, and therefore a steeper LF. We hope to address some of these issues in the future.

Acknowledgements. We are grateful to Helmuth Kristen for obtaining a few images of the cluster in September 1995 and to Steven Jörsäter for some initial observations in 1994. We also thank Leif Festin for supplying some ALFOSC images that we could use to test the image quality prior to our observations. We are grateful to Margrethe Wold for discussions about completeness and to Tomas Dahlén for discussions and assistance with an additional consistency check. We also thank the referee, C. Gronwall, who provided several important suggestions that improved the presentation of this work. Last but not least, M. N. is very grateful to Stefan Larsson for discussions about statistics and related topics. The data presented here have been taken using ALFOSC, which is owned by the Instituto de Astrofisica de Andalucia (IAA) and operated at the Nordic Optical Telescope under agreement between IAA and the NBIfA of the Astronomical Observatory of Copenhagen. This research was supported by the Swedish Natural Sciences Research Council, and the Göran Gustafsson Foundation for Research in Natural Sciences and Medicine.

References

Arnouts S., D'Odorico S., Cristiani S., Zaggia S., Fontana A., Giallongo E., 1999, A&A 341, 641
Bahcall J. N., 1995, http://www.sns.ias.edu/~ jnb/Html/galaxy.html
Bahcall, J. N., Soneira, R. M. , 1980, ApJS, 44, 73
Bernstein, G. M., Nichol, R. C., Tyson, J. A., Ulmer, M. P., Wittman, D. 1995, AJ, 110, 1507 (BNTUW)
Binggeli B., Sandage A., Tammann G. A., 1988, ARA&A 26, 509
Biviano, A., Durret, F., Gerbal, D., Le Fevre, O., Lobo, C., Mazure, A. & Slezak, E., 1995, ApJ, 455, 108
Baugh, C.M., Cole, S. & Frenk, C. S. 1996, MNRAS, 283, 1361
Bohlin, R. C., Savage, B. D., Drake, J. F. 1978, ApJ, 224, 132B
Bothun G. D., Impey C. D., Malin D. F., 1991, ApJ 376, 404
Burstein, D., Heiles, C. 1982, AJ, 87, 1165
Butcher H., Oemler A.. 1984, ApJ, 285, 426
Davies J. I., Disney M. J., Phillipps S., Boyle B. J., Couch W. J., 1994, MNRAS 269, 349
Driver, S. P., 1999, ApJ 526, L69
Driver, S. P., Phillipps, S., Davies, J. I., Morgan, I., and Disney, M. J. 1994a, MNRAS 266, 155
Driver, S. P., Phillipps, S., Davies, J. I., Morgan, I., Disney, M. J. 1994b, MNRAS 268, 393 (DPDMD)
Driver, S. P., Couch W. J., Phillipps, S., Smith R., 1998, MNRAS 301, 357
Ellis, R. S., Colless, M., Broadhurst, T., Heyl, J., Glazebrook, K. 1996, MNRAS, 280, 235
Ferguson H. C., Binggeli B., 1994, A&AR 6, 67
Ferguson H. C., Sandage A., 1988, AJ 96, 1520
Fontana A., D'Odorico S., Fosbury R., Giallongo E., Hook R., Poli F., Renzini A., Rosati P., Viezzer R., 1999, A&A 343, L19
Gioia, I.M. & Luppino, G.A. 1994, ApJ Suppl, 94, 583
Gioia, I. M., Maccacaro, T., Schild, R. E., Wolter, A., Stocke, J. T., Morris, S. L., Henry, J. P. 1990, ApJS, 72, 567
Gronwall, C. & Koo, D. C. 1995 ApJ, 440, L1
Heyl, J. S., Cole, S., Frenk, C. S., Navarro, J. F. 1995, MNRAS, 274, 755
Impey C., Bothun G., Malin D., 1988, ApJ 330, 634
Impey C., Bothun G., 1997, ARA&A 35, 267
Jarvis J. F., Tyson J. A., 1981, AJ 86, 476
Kaufmann, G. 1995a, MNRAS, 274, 153
Kaufmann, G. 1995b, MNRAS, 274, 161
Kaufmann, G., White, S. D. M., Guiderdoni, B. 1993, MNRAS, 264, 201
Lilly, S. J., Tresse, L., Hammer, F., Crampton, D. Le Fevre, O. 1995, ApJ, 455, 108

Lobo, C., Biviano, A., Durret, F., Gerbal, D., LeFevre, O., Mazure, A., Slezak, E. 1997, A&A 317, 385
Loveday, J., Peterson, B. A., Efstathiou, G., Maddox, S. J. 1992, ApJ, 390, 338
Marzke, R. O., Geller, M. J., Huchra, J. P., Corwin, H. G., Jr. 1994b, AJ 108, 437
McGaugh S. S., Bothun G. D., 1994, AJ 107, 530
Metcalfe, N., Fong, R., Shanks, T., & Jones, L.R. 1991, MNRAS, 249, 498
Moore B., Katz N., Lake G., Dressler A., Oemler A., 1996, Nat 379, 613
Näslund M., 1995, Licentiate thesis, Stockholm Observatory, Stockholm University
Näslund M., 1998, Ph. D. thesis, Stockholm Observatory, Stockholm University (the part dealing with the simulations can be found at http://www.astro.su.se/~ magnus/research/publications.html)
Propris, R. de, Pritchet, C. J., Harris, W. E., McClure, R. D., 1995, ApJ, 450, 534
Schlegel D.J., Finkbeiner D.P., Davis M., 1998, ApJ, 500, 525
Smith R. M., Driver S. P., Phillipps S., 1997, MNRAS 287, 415
Sprayberry D., Impey C. D., Bothun G. D., Irwin M. J., 1995, AJ 109, 558
Stetson, P. B., 1987, PASP 99, 191
Stocke, J. T., Morris, S. L., Gioia, I. M., Maccacaro, T., Schild, R., Wolter, A., Fleming, T. A., Henry, J. P. 1991, ApJS, 76, 813
Thompson L. A., Gregory S. A., 1993, AJ 106, 2197
Trentham N., 1997, MNRAS 286, 133
Trentham N., 1998a, MNRAS 293, 71
Trentham N., 1998b, MNRAS 294, 193
Trentham N., 1998c, MNRAS 294, 193
Trentham N., 1998d, preprint (astro-ph/9804013)
Trentham N., Mobasher B.,1998, MNRAS 299, 488
Tyson, J.A. 1988, AJ, 96, 1
Valdes F., 1982, *Faint Object Classification and Analysis System*, NOAO, Tucson, AZ
Valdes F., 1993, *FOCAS User's Guide*, NOAO, Tucson, AZ
Valotto C. A., Nicotra M. A., Muriel H., Lambas D. G., 1997, ApJ 479, 90
White S. D. M., Frenk, C. S. 1991, ApJ 379, 52
White S. D. M., Springel V., 1999, preprint (astro-ph/9911378)
Wilson G., Smail I., Ellis R. S., Couch W. J. 1997, MNRAS, 284, 915 (WSEC)

This figure "fig1.jpg" is available in "jpg" format from:

http://arXiv.org/ps/astro-ph/0002372v1

This figure "fig2.jpg" is available in "jpg" format from:

http://arXiv.org/ps/astro-ph/0002372v1

This figure "fig3.gif" is available in "gif" format from:

http://arXiv.org/ps/astro-ph/0002372v1